NANO LETTERS

Letter

pubs.acs.org/NanoLett

Optofluidic Concentration: Plasmonic Nanostructure as Concentrator and Sensor

Carlos Escobedo,[†] Alexandre G. Brolo,[‡] Reuven Gordon,[§] and David Sinton[∥,*]

[†]Department of Biosystems Science and Engineering, Bio Engineering Laboratory, ETH Zurich, Mattenstrasse 26, CH-4058 Basel, Switzerland

[‡]Department of Chemistry, University of Victoria, P.O. Box 3065, Victoria, British Columbia, V8W 3V6, Canada

[§]Department of Electrical and Computer Engineering, University of Victoria, P.O. Box 3055, Victoria, British Columbia, V8W 3P6, Canada

[∥]Mechanical and Industrial Engineering, University of Toronto, 5 King's College Road, Toronto, Ontario, M5S 3G8, Canada

S *Supporting Information*

ABSTRACT: The integration of fluidics and optics, as in flow-through nanohole arrays, has enabled increased transport of analytes to sensing surfaces. Limits of detection, however, are fundamentally limited by local analyte concentration. We employ the nanohole array geometry and the conducting nature of the film to actively concentrate analyte within the sensor. We achieve 180-fold enrichment of a dye, and 100-fold enrichment and simultaneous sensing of a protein in less than 1 min. The method presents opportunities for an order of magnitude increase in sensing speed and 2 orders of magnitude improvement in limit of detection.

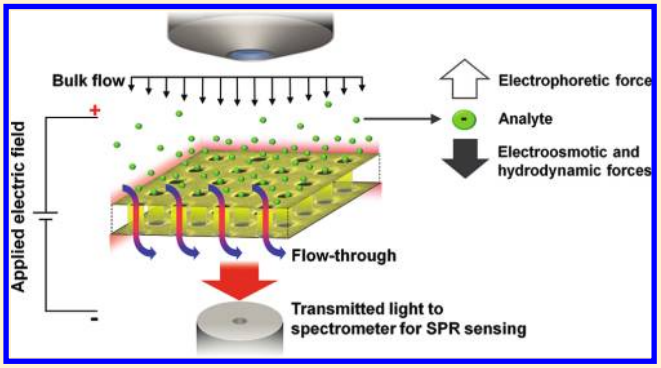

KEYWORDS: *Nanoholes, surface plasmon, flow-through, optofluidics, plasmonics, analyte enrichment, electric field gradient focusing*

The marriage of fluidics and optics, or optofluidics, has enabled new functionality in several areas including analytical chemistry, biotechnology, and energy.[1−6] While arrays of nanoholes in metal films have been used for surface plasmon based sensing for several years,[7] incorporating the nanoholes as fluidic nanochannels has resulted in improved sensor response.[8] The key benefit in that optofluidic approach is improved transport, and several studies have confirmed and extended the concept.[9−13]

Despite the benefits of improved analyte transport and established optical sensitivity, applicability of optofluidic sensing systems is limited in many applications by low target analyte concentrations.[14,15] Specifically for the early detection of many diseases, such as ovarian cancer, biomarker concentrations remain low until late stages.[16] Current methods to concentrate analyte prior to sensing include field amplified stacking,[17] isotachophoresis,[18] electrokinetic trapping,[19,20] conductivity gradient focusing,[21] temperature gradient focusing[22] and electric field gradient focusing (EFGF).[23] EFGF may be achieved in a microchannel using a floating internal electrode;[24] thus, there is an opportunity to apply this approach with metallic flow-through nanohole arrays. In traditional EFGF, concentration results from a steep field gradient in a microchannel containing a buffer and a floating electrode.[25,26] The electrode disturbs the potential field, and the balance of local electrokinetic transport and bulk flow results in the local collection of charged species (e.g., buffer ions and charged analytes).[24] The net concentration increase results from a combination of EFGF, diffusion, bulk fluid transport, and secondary influences of induced-charge electrokinetics[27,28] (details provided in the Supporting Information).

In this work, we present a plasmonic nanostructure that locally concentrates analyte prior to sensing. The flow-through nanohole array sensor operates as a floating electrode when an electric potential is applied to the fluid. A combination of EFGF and bulk pressure-driven flow bias concentrates analyte at the active sensing surface. The result is a straightforward experimental approach that enables the use of the plasmonic structure as both analyte concentrator and sensor.

Figure 1 outlines the optofluidic concentration approach as a combination of electrohydrodynamic effects. An array of through nanoholes is integrated within a microfluidic system. The fluid is a typical buffer with many small ions and larger electrically charged analytes (here, negatively charged). Concentrations are initially uniform throughout the system. The application of an electric field results in a bulk electroosmotic flow toward the cathode, and electrophoretic motion of cations and anions toward the cathode and anode,

Received: December 21, 2011
Revised: February 19, 2012
Published: February 21, 2012

   dx.doi.org/10.1021/nl204504s | *Nano Lett.* 2012, 12, 1592−1596

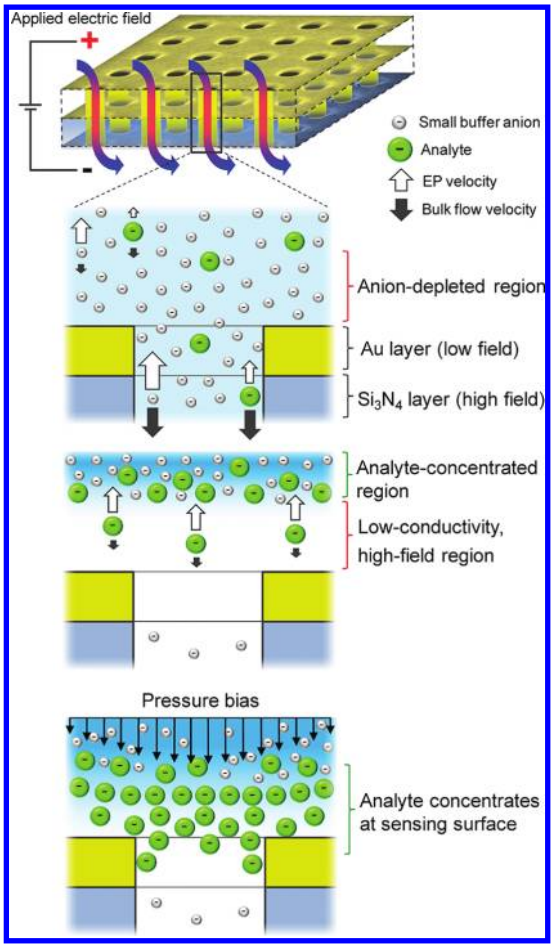

Figure 1. Optofluidic concentration approach showing additive effects. A through nanohole array in a metallic film is embedded in a microfluidic environment containing analyte in buffer. Concentrations are uniform everywhere prior to the application of the electric field. Small buffer anions have high electrophoretic velocities sufficient to counter the bulk flow everywhere except inside the metallic portion of each nanohole where the electric field strength is reduced. An anion-depleted region next to the Au layer of the nanohole array develops. Larger charged analytes respond to the locally increased field and concentrate near the boundary of the depleted region. In combination with a pressure bias, the position of the concentrated analyte plug is shifted down to the nanohole array surface and into the holes where it can be sensed at high concentration as compared to the initial sample.

respectively. Small buffer anions have high electrophoretic velocities sufficient to counter the bulk flow everywhere except inside the metallic portion of each nanohole where the electric field strength is locally reduced (Figure 1). This effect results in a local depletion of buffer anions, which grows toward the anode as the local conductivity reduces and the local electric field magnitude increases, typical of EFGF.[24] The time scale for this buffer ion response is ~1 ms (details provided in the Supporting Information). Larger charged analytes respond to the increased field and concentrate near the boundary of the depleted region (Figure 1). In combination with a pressure bias, the position of the concentrated analyte plug is shifted down to the nanohole array surface and into the holes where it can be sensed at greatly elevated concentrations as compared to the initial sample.

We used arrays of 300 nm diameter through-holes with 450 nm periodicity fabricated in 100 nm-thick Si_3N_4 membranes coated with a 100 nm Au film. Each nanohole array was 100 μm^2. The arrays were integrated within a microfluidic system containing 1:1 (v/v) methanol/10 mM Tris-HCl solution (pH 8.1) seeded with model analyte, and electrodes (details of the set up provided in the Supporting Information). The experiments included two model analytes: fluorescein, for quantifying the concentration effect, and bovine serum albumin (BSA) for concurrent analyte concentration and sensing. In the sensing experiments, the incident laser light spot was confined to $D \sim 100$ μm such that only a single nanohole array was interrogated, and transmitted light was collected from the silicon nitride side (details in Supporting Information).

Figure 2 shows results of optofluidic concentration experiments using a charged dye. For quantifying the concentration effect, a substrate with flow-through nanohole arrays was visualized from the Au side, as shown in Figure 2a. Initially, the dilute dye concentration (100 nM fluorescein) was uniform throughout the whole system ($t = t_0$ in Figure 2b). At $t = t_1 =$ 15 s, a potential of 50 V is applied externally, and the concentration increases steadily as fresh analyte is transported to the arrays by the bulk pressure driven flow (4 kPa). As time progresses the charged dye is locally concentrated on the anodic side (visualized) surrounding the nanohole arrays and a depleted region is developed near the arrays (a movie of the experiment is available in the Supporting Information). As shown in Figure 2c, the local enrichment process showed an approximately linearly increasing trend over time, reaching a concentration factor of ~180-fold in 60 s. As with similar EFGF techniques, the ultimate limit of the concentration effect is governed by a balance of bulk flow, electrophoresis, and diffusion.[24,29−31] With the analyte solution, geometry, and flow rates applied here, the concentration is expected to plateau on the order of minutes in keeping with related systems.[24,26] This limit was not observed here prior to saturation of the detector shortly after $t = 1$ min. The collection rate in Figure 2c corresponds to the incoming flow rate of dye, over an area of 30 × 30 μm on the top-left array, indicating that the bulk of the model analyte is being concentrated on the gold, active sensing side. To increase the rate of analyte collection the applied pressure and voltage can be increased to the practical limits. The applied voltage is limited by the onset of electrolysis that disrupts the process and can block the nanoholes with vapor bubbles. Local electrolysis at the nanohole arrays was found to occur at applied voltages above 70 V with this setup. The pressure is limited only by the mechanical properties of the membrane: deformation increases with pressure, which alters the position of the arrays, and breakage occurs at pressures above ~150 kPa for these structures. The running parameters employed here ensured no local electrolysis and negligible deformation of the membrane.

The previous experimental setup was reoriented in order to visualize the process from the downstream cathodic compartment of the cell, as illustrated in Figure 2d. Observation from the backside was required to confirm that the charged analyte is concentrated on the gold side by preventing charged analytes from passing through the nanohole arrays. A sequence of processed fluorescence images of the experiment is shown in Figure 2e. With the application of the electric field, significant fluorescence in the nanoholes appears ($t = t_1 = 60$ s). Over the subsequent 60 s, ($t = t_2 = 120$ s), the local intensity at the arrays continues to increase. The four bright spots surrounding each nanohole array are reflections from the silicon frame that supports the membrane and are simply artifacts from imaging the backside of the assembly. The surface plots corresponding

dx.doi.org/10.1021/nl204504s | Nano Lett. 2012, 12, 1592−1596

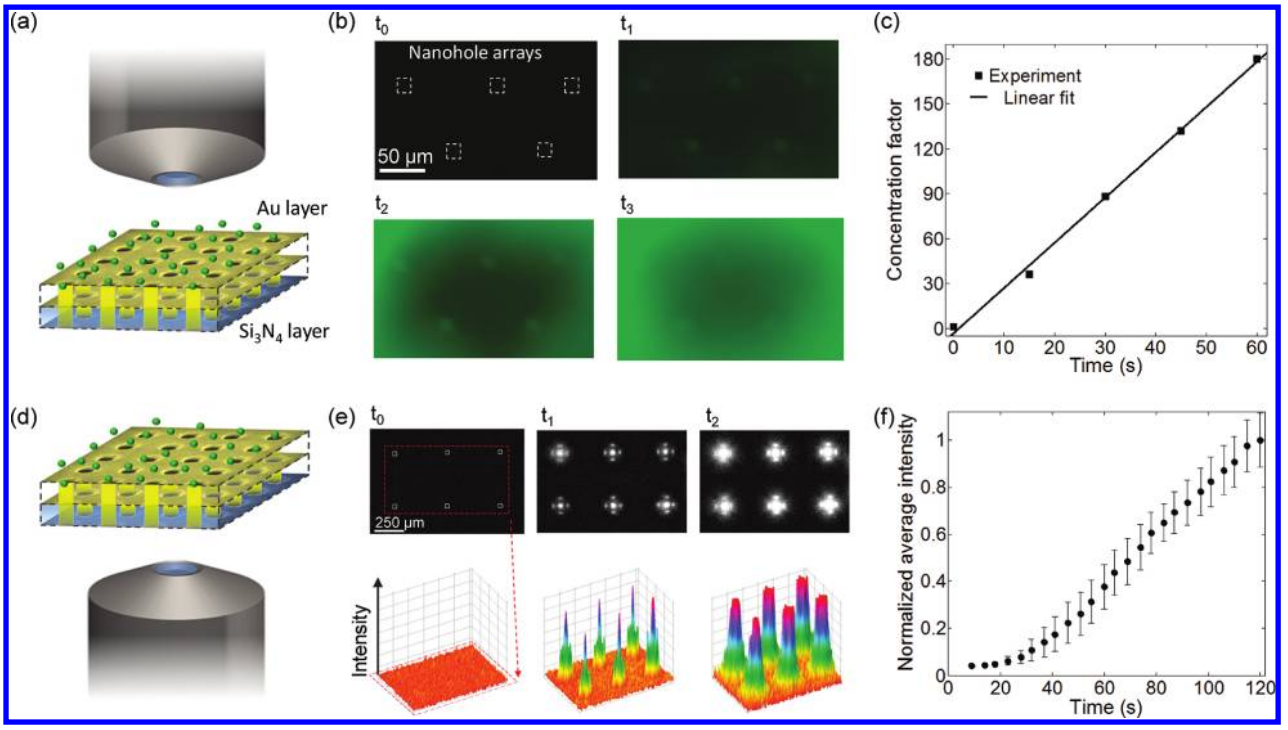

Figure 2. Optofluidic concentration of fluorescein. (a) Schematic of the experiment visualizing fluorescein concentration from the gold side (anode chamber). (b) Image sequence during the optofluidic concentration process (50 V and 4 kPa applied; 4 images at 15 s intervals) in an Au-on-Si_3N_4 membrane with five nanohole arrays. (c) Concentration enrichment plot over time (top-left array). (d) Schematic of the experiment visualizing fluorescein concentration from the silicon nitride side (cathode chamber). A six-window Si_3N_4 membrane with a nanohole array in each window was used. The initial fluorescein concentration, array geometries, and applied voltage and pressure were the same as those in panel b. (e) Image sequence showing the progress of fluorescein concentration at the Au side of the nanohole arrays (no voltage at $t = t_0$). Surface plots corresponding to each image show the evolution of the local fluorescence signal collected from each nanohole array. (f) Plot of the local fluorescence intensity as a function of time over an area of 30 × 30 pixels. The vertical bars indicate the standard deviation.

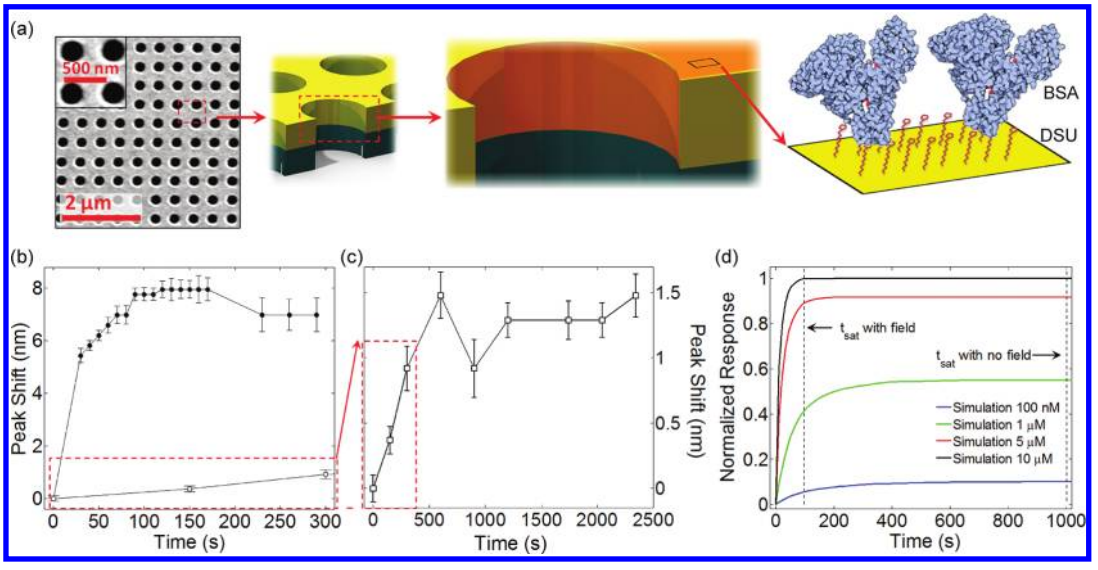

Figure 3. (a) Illustration of BSA binding on the functionalized active surface of the optofluidic sensor. (b) Resonance peak-shift monitoring of BSA binding to DSU under both active concentration (50 V, 4 kPa) and control conditions (no applied field). With the applied field, the peak-shift reached a plateau after ~120 s. The control experiment shows a slower binding rate without reaching saturation within the time range in this figure. (c) Resonance peak-shift monitoring during BSA binding under control conditions (no applied field). The time required to reach equilibrium was 10-fold compared to the concentration scheme, and the magnitude of the shift was 5-fold smaller. Error bars indicate the standard deviation of the mean peak shift. (d) Simulated sensor response (BSA binding) using different BSA concentrations. The saturation times, t_{sat}, from both experiments (with and without the electric field) are shown as vertical dashed lines. The saturation time for the optofluidic concentration experiment agrees with the 10 μM simulation curve. This indicates that the concentration scheme developed here enabled local sensing of the analyte with concentration 100-fold greater than the solution employed.

dx.doi.org/10.1021/nl204504s | *Nano Lett.* 2012, 12, 1592–1596

to each image in Figure 2e show the evolution of the local fluorescence signal collected from each nanohole array. The increasing localized signal and lack of dye transport (i.e., no dye streaming) into the lower layer[8] indicate (1) the analyte concentration effect on the gold side and (2) the presence of concentrated analyte inside the nanoholes that absorb and emit in response to direct excitation from below. The plot in Figure 2f shows the local fluorescence intensity as a function of time. An integration area of 30 × 30 pixels was selected over each array, and excluded the four reflection artifacts. Because of the intense confinement of the analyte within the holes, and further complexities of fluorescence imaging within and through the nanoholes, it is not possible to directly obtain concentration factors from this bottom-side imaging configuration for comparison with that measured on the gold side. However, several aspects of the normalized intensity plot in Figure 2e are notable: (1) the signal increase occurs primarily after 40 s, which corresponds approximately to the t_2 to t_3 period in Figure 2b where the local concentration at the arrays increases significantly; (2) after 40 s, the observed intensity shows a linear increasing trend; (3) the rate of normalized intensity increase is on the same order as that observed in the gold-side chamber. Collectively, these fluorescence imaging results provide insight into the transport phenomena and confirm active analyte concentration on the gold side of the nanostructure. In the context of sensing applications, however, surface-bound analyte concentration and the corresponding sensor response are the ultimate performance metrics for a concentration strategy.

The model sensing experiment involved electrohydrodynamic concentration and subsequent nonspecific detection of BSA (with isoelectric point of 4.7 at room temperature[32]). Sensing was achieved by tracking the peak-shift of the light transmission spectrum at the resonant wavelength[7] (details in the Supporting Information). This experiment was designed to quantify and contrast the rate of biomolecular binding with and without the active concentration method developed here. Figure 3a shows a schematic representation of the system with BSA binding to the surface of the nanohole arrays. The plot in Figure 3b shows the experimental results using the analyte concentration scheme at an applied electric potential of 50 V. The data for the control case (no field applied) is shown in Figure 3b for the first 300 s and Figure 3c for the subsequent 1500 s, followed by a final rising step at t = 1600 s. The peak-shift indicates the binding of BSA to DSU on the sensing surface of the optofluidic nanostructure as time progresses. The peak-shift change over time shows the typical surface binding characteristic shape, reaching saturation of the sensing surface after ∼120 s for the concentration experiment (with field) in Figure 3a. The small blue-shift on the order of 1 nm after the rinse step confirms the formation of a BSA-DSU layer on the surface of the sensor. The magnitude of the peak-shift for the control case, shown in Figure 3c, is small (∼1.5 nm) and the time for reaching equilibrium is long (in the order of ∼1000 s), which is in contrast to the shift obtained in the concentration scheme (shown in Figure 3b). In combination, these results demonstrate that the concentration scheme developed here enabled a 10-fold decrease in binding time, and a 5-fold increase in peak shift. These differences correlate to the expected concentration-dependence of the binding kinetics.[33] In other words, the faster saturation and increased magnitude in peak-shift obtained with the analyte concentration scheme is consistent with the locally increased analyte concentration in the fluid resulting from the optofluidic concentration method.

To contextualize the sensing results, we developed a computational model including transport and reaction kinetics but excluding the active concentration effect (further details in the Supporting Information). The binding of the model analyte, BSA, to DSU is nonspecific and is described by simple first-order reaction kinetics.[34] In this type of kinetics, the maximum amount of bound analyte at the active surface of the sensor is characterized by the equilibrium time constant, τ, which depends on the local concentration of the analyte (additional details can be found in the Supporting Information). The model was applied to predict the response of the sensor for local analyte concentrations spanning from 100 nM to 10 μM. In order to compare rates, the responses were normalized to the equilibrium value for the maximum concentration (10 μM). As shown in Figure 3d, adsorption rates increase with increased concentration, as expected. As the response corresponds to the amount of analyte bound to the sensing surface, the response is smaller for the low concentrations, which is in agreement with the experimental results. The saturation time for the experimental results with active concentration (shown as a vertical dashed line) agrees most closely to the 10 μM bulk analyte concentration response curve (a concentration 100-fold that of the initial concentration). These results indicate that the optofluidic concentration scheme developed here enabled sensing of an analyte with response corresponding to a bulk concentration 100-fold greater than the solution employed. In the context of limits of detection, nanohole arrays can operate at signal-to-noise ratios (SNRs) over 800 and detect antibody concentrations down to 1 nM.[35] With active local concentration as demonstrated here, this limit could in principle be extended 2 orders of magnitude into the ∼10 pM range using the same nanostructures. Importantly, the concentration method is not restricted to nanohole arrays and is applicable more generally to sensors involving holes or pores in a metal film, such as zero mode waveguides[36,37] and nanopore-based single-molecule detection.[38,39]

We demonstrated active analyte concentration and sensing using a flow-through plasmonic nanostructure. Metallic flow-through nanohole arrays served as both floating electrodes and nanochannels that under an externally applied voltage and a hydrostatic pressure bias enabled the local concentration of analytes. We also demonstrate the concurrent use of the flow-through optofluidic nanostructure to concentrate a protein and to sense its binding to a functionalized Au nanohole surface. The results from this sensing experiment in combination with computational simulations indicated a 100-fold analyte concentration as compared to the control case with no concentrating effect. Collectively, these results indicate an order of magnitude increase in sensing speed and 2 orders of magnitude improvement in limit of detection.

■ ASSOCIATED CONTENT

Ⓢ Supporting Information

Additional information on the nanohole array fabrication, the experimental setup integration and fabrication, chemicals and solutions preparation, fluorescein quantification and sensing experiments procedure, and the BSA binding kinetics simulations. This material is available free of charge via the Internet at http://pubs.acs.org.

dx.doi.org/10.1021/nl204504s | Nano Lett. 2012, 12, 1592−1596

AUTHOR INFORMATION

Corresponding Author

*E-mail: sinton@mie.utoronto.ca. Phone: (416) 978-1623. Fax: (416) 978-7753.

Notes

The authors declare no competing financial interest.

ACKNOWLEDGMENTS

The authors gratefully acknowledge the financial support to the Natural Sciences and Engineering Research Council of Canada, NSERC, through a scholarship to C.E. and research grant in partnership with the BC Cancer Agency Trev and Joyce Deeley Antibody Research Unit and Micralyne Inc. Funding from the Canada Research Chairs Program, the Canada Foundation for Innovation, and the British Columbia Knowledge Development Fund are also gratefully acknowledged.

REFERENCES

(1) Psaltis, D.; Quake, S. R.; Yang, C. H. *Nature* **2006**, *442* (7101), 381−386.
(2) Schmidt, H.; Hawkins, A. R. *Nat. Photonics* **2011**, DOI: 10.1038/nphoton.2011.163.
(3) Fan, X.; White, I. M. *Nat. Photonics* **2011**, DOI: 10.1038/nphoton.2011.206.
(4) Shahi, S. *Nat. Photonics* **2010**, *4* (5), 269−269.
(5) Cuennet, J. G.; Vasdekis, A. E.; De Sio, L.; Psaltis, D. *Nat. Photonics* **2011**, *5* (4), 234−238.
(6) Erickson, D.; Sinton, D.; Psaltis, D. *Nat. Photonics* **2011**, DOI: 10.1038/nphoton.2011.209.
(7) Anker, J. N.; Hall, W. P.; Lyandres, O.; Shah, N. C.; Zhao, J.; Van Duyne, R. P. *Nat. Mater.* **2008**, *7* (6), 442−453.
(8) Eftekhari, F.; Escobedo, C.; Ferreira, J.; Duan, X.; Girotto, E. M.; Brolo, A. G.; Gordon, R.; Sinton, D. *Anal. Chem.* **2009**, *81* (11), 4308−4311.
(9) Yanik, A. A.; Huang, M.; Kamohara, O.; Artar, A.; Geisbert, T. W.; Connor, J. H.; Altug, H. *Nano Lett.* **2010**, *10* (12), 4962−4969.
(10) Ferreira, J.; Santos, M. J. L.; Rahman, M. M.; Brolo, A. G.; Gordon, R.; Sinton, D.; Girotto, E. M. *J. Am. Chem. Soc.* **2009**, *131* (2), 436−437.
(11) Zhang, D. Y.; Men, L. Q.; Chen, Q. Y. *Sensors* **2011**, *11* (5), 5360−5382.
(12) Guo, Y. B.; Li, H.; Reddy, K.; Shelar, H. S.; Nittoor, V. R.; Fan, X. D. *Appl. Phys. Lett.* **2011**, *98*, 041104.
(13) Escobedo, C.; Vincent, S.; Choudhury, A. I. K.; Campbell, J.; Brolo, A. G.; Sinton, D.; Gordon, R. *J. Micromech. Microeng.* **2011**, *21* (11), 115001 DOI: 10.1088/0960-1317/21/11/115001.
(14) Wang, Y. C.; Han, J. Y. *Lab Chip* **2008**, *8* (3), 392−394.
(15) Sinton, D.; Gordon, R.; Brolo, A. G. *Microfluid. Nanofluid.* **2008**, *4* (1−2), 107−116.
(16) Buchen, L. *Nature* **2011**, *471* (7339), 428−432.
(17) Sustarich, J. M.; Storey, B. D.; Pennathur, S. *Phys. Fluids* **2010**, *22*, 112003.
(18) Jung, B.; Bharadwaj, R.; Santiago, J. G. *Anal. Chem.* **2006**, *78* (7), 2319−2327.
(19) Wang, Y. C.; Stevens, A. L.; Han, J. Y. *Anal. Chem.* **2005**, *77* (14), 4293−4299.
(20) Kim, S. J.; Han, J. Y. *Anal. Chem.* **2008**, *80* (9), 3507−3511.
(21) Shackman, J. G.; Ross, D. *Electrophoresis* **2007**, *28* (4), 556−571.
(22) Ross, D.; Locascio, L. E. *Anal. Chem.* **2002**, *74* (11), 2556−2564.
(23) Koegler, W. S.; Ivory, C. F. *Biotechnol. Prog.* **1996**, *12* (6), 822−836.
(24) Hlushkou, D.; Perdue, R. K.; Dhopeshwarkar, R.; Crooks, R. M.; Tallarek, U. *Lab Chip* **2009**, *9* (13), 1903−1913.
(25) Dhopeshwarkar, R.; Hlushkou, D.; Nguyen, M.; Tallarek, U.; Crooks, R. M. *J. Am. Chem. Soc.* **2008**, *130* (32), 10480−10481.
(26) Piruska, A.; Branagan, S.; Cropek, D. M.; Sweedler, J. V.; Bohn, P. W. *Lab Chip* **2008**, *8* (10), 1625−1631.
(27) Bazant, M. Z.; Squires, T. M. *Phys. Rev. Lett.* **2004**, *92* (6), 066101.
(28) Gamayunov, N. I.; Mantrov, G. I.; Murtsovkin, V. A. *Colloid J. USSR* **1992**, *54* (1), 20−23.
(29) Koegler, W. S.; Ivory, C. F. *Journal of Chromatography A* **1996**, *726* (1−2), 229−236.
(30) Anand, R. K.; Sheridan, E.; Hlushkou, D.; Tallarek, U.; Crooks, R. M. *Lab Chip* **2011**, *11* (3), 518−527.
(31) Kelly, R. T.; Woolley, A. T. *J. Sep. Sci.* **2005**, *28* (15), 1985−1993.
(32) Böhme, U.; Scheler, U. *Chem. Phys. Lett.* **2007**, *435* (4−6), 342−345.
(33) Squires, T. M.; Messinger, R. J.; Manalis, S. R. *Nat. Biotechnol.* **2008**, *26* (4), 417−426.
(34) Gervais, T.; Jensen, K. F. *Chem. Eng. Sci.* **2006**, *61* (4), 1102−1121.
(35) Im, H.; Sutherland, J. N.; Maynard, J. A.; Oh, S.-H. *Anal. Chem.* **2012**, DOI: 10.1021/ac300070t.
(36) Levene, M. J.; Korlach, J.; Turner, S. W.; Foquet, M.; Craighead, H. G.; Webb, W. W. *Science* **2003**, *299* (5607), 682−686.
(37) Miyake, T.; Tanii, T.; Sonobe, H.; Akahori, R.; Shimamoto, N.; Ueno, T.; Funatsu, T.; Ohdomari, I. *Anal. Chem.* **2008**, *80* (15), 6018−6022.
(38) Singer, A.; Wanunu, M.; Morrison, W.; Kuhn, H.; Frank-Kamenetskii, M.; Meller, A. *Nano Lett.* **2010**, *10* (2), 738−742.
(39) Venkatesan, B. M.; Bashir, R. *Nat. Nanotehcnol.* **2011**, *6* (10), 615−624.